

Semi-classical evaporative cooling: classical and quantum distributions

A. A. Arvizu-Velazquez

*Centro de Investigación en Computación, Instituto Politécnico Nacional,
Av. Luis Enrique Erro S/N, Unidad Profesional Adolfo López Mateos,
Zacatenco, Alcaldía Gustavo A. Madero, C.P. 07738, Ciudad de México.**

A. A. del Río-Lima

*Instituto de Química, Universidad Nacional Autónoma de México,
Apartado Postal 20-364, 01000 Ciudad de México, México*

S. Dondé-Rodríguez

Instituto de Física, Universidad Nacional Autónoma de México, C.P. 04510, México

F.J. Poveda-Cuevas

*Investigador por México - Instituto de Física,
Universidad Nacional Autónoma de México, C.P. 04510, México*

(Dated: March 24, 2026)

A unified semiclassical framework is presented to describe the evaporative cooling of trapped atomic gases, accounting for both classical and quantum statistics. By combining global thermodynamics with phase-space distributions, general analytic expressions for the particle number and internal energy are derived for a broad family of confining potentials. Building on these results, a recursive evaporation protocol is formulated based on truncated energy distributions, enabling stepwise mapping between successive thermodynamic states and revealing the system's degree-of-freedom governance over cooling efficiency. Numerical simulations of the systems highlight the contrasting behavior of classical and quantum systems as they approach degeneracy, with particularly distinctive signatures in quadrupole traps, due to their nonstandard phase-space scaling. The results provide a versatile theoretical tool for modeling evaporative cooling across experimentally relevant geometries and offer quantitative guidance for optimizing cooling trajectories in ultracold atomic systems.

* Also at Facultad de Ciencias, Universidad Nacional Autónoma de México, Alcaldía Coyoacán, C.P. 04510 Ciudad Universitaria, Ciudad de México, México

I. INTRODUCTION

Evaporation in trapped atomic gases is the cornerstone to achieving fermionic [1] and bosonic [2–4] quantum degeneracy. The goal in the experimental community is to achieve the optimal balance between evaporation rate and conservation of atomic number. A large number of particles and low temperature often determine the signal-to-noise ratio, which is crucial for conducting control experiments and for quantum simulators. The optimal evaporation parameters are typically resolved through artisanal processes, as they depend strongly on experimental conditions and prior cooling, including trap depth, potential geometry, and chamber vacuum. A thermodynamic description is more viable because the quantities are measured directly within an experimental sequence. In addition, it models the adiabatic process along the evaporation path very well, which is usually difficult to model from a microscopic perspective [5, 6] or within kinetic theory [7, 8].

The production of samples at ultracold temperatures has generated significant interest in studying the physics of quantum phenomena, including atomic collisions, superfluidity, and degenerate quantum gases. The rapid development of experimental and theoretical studies of ultracold trapped gases has significantly increased our understanding of these thermodynamic systems. This work contributes to an ongoing effort to control and manipulate quantum systems with potential technological applications in multiple fields [9–11]. The versatility and fine control of external parameters achievable by quantum gases are relevant [12, 13].

On the other hand, the key to the potential engineering of quantum gases lies in the domain of light-matter interaction. Light parameters such as intensity, frequency, phase, and detuning can have observable effects on ultracold or quantum gases, e.g., by enabling the creation of focused optical potentials that serve as conservative traps [14]. Thus, for far-red detuning, the atoms will suffer an attractive force towards the center of the trap [4, 15, 16], while if the out-of-tune is towards blue, the resulting potential will be repulsive [17, 18]. Therefore, this important property can be used as an advantage since it is possible to create any potential with the characteristics of interest [19, 20].

Given the ability to experimentally create any external potential, this work presents the following configurations: a 3D box, a 2D box plus a 1D harmonic oscillator (HO), a 1D box plus a 2D HO, a 3D HO, and the Quadrupolar potential. The mixed cases are considered in this work, as it is known that the experimental realization of external traps that combine harmonic with box-type potentials has been important in the approach to two-dimensional physics, as they have been obtained for both Bose [21, 22] and Fermi gases [23, 24].

Another important aspect of this work is that atomic gases are confined in magnetic and electric fields, rather than contained in a rigid-walled vessel. As a consequence, the thermodynamics describing the state of

the system needs to be reformulated in terms of new global thermodynamic variables [25, 26] that consider the definition of extensive quantities that do not depend on the volume of a vessel, but on some potential parameters, in concordance with experimental approaches [27–29].

The article is structured as follows: Section II provides a brief overview of global thermodynamics and the semiclassical distribution. Section III outlines the protocol for evaporating a cloud within a trap. Finally, Section IV presents the numerical results and their connections to experimental implementations.

II. THERMODYNAMICS OF TRAPPED ATOMIC GASES

A. The Ideal Gas Limit

Before the evaporative cooling process of any ultracold atomic gas, the system can be described as an ensemble of N interacting classical particles at sufficiently high temperatures. Thus, the complete description is given by the position and momentum coordinates of each particle $\{\mathbf{r}_i, \mathbf{p}_i\}$, which defines a state of the system in the six-dimensional phase space.

In general, interactions between particles are described through an interatomic central potential $\mathcal{V}(\mathbf{r}_i - \mathbf{r}_j)$. Interactions affect the thermodynamics and kinetics of the gas, which determine the time required to reach thermal equilibrium. However, depending on the comparison of certain characteristic lengths, such as the range interaction r_0 and the interparticle distance $n_0^{-1/3}$ of the gas with density n_0 , the effective interaction potential can be approximated to recover the important characteristics of the system.

If the interparticle distance is much greater than the interaction range, $n_0 r_0^3 \ll 1$, the atomic gas is said to be in the dilute regime. Thus, the gas is governed by binary interactions, since the probability of finding three atoms within a distance r_0 of each other is extremely low and negligible.

Moreover, the collision rate depends on the atom's size, as characterized by the cross-section. The kinetic diameter of an atom is approximately equal to the range of the interaction potential; this gives us an estimate for the binary cross-section of the atom: $\sigma = \pi r_0^2$, for the mean free path $l^{-1} = n\sigma$, and for the collision rate: $\tau_c^{-1} = n\sigma\bar{v}_r$, where $\bar{v}_r = \sqrt{16k_B T/\pi m}$ is the average relative atomic speed.

By comparing the atomic mean free path with the size of the gas cloud, two density regimes are distinguished: a low-density regime where the mean free path exceeds the size of the cloud ($l \gg V^{1/3}$) and a high-density regime where the size of the cloud exceeds the mean free path ($l \ll V^{1/3}$). In a low-density regime, the gas is referred to as collisionless; in the opposite, the gas is referred to as hydrodynamic.

By controlling the conditions in atomic-physics experiments, the system can be brought into the collisionless regime. Furthermore, at the beginning of the evaporative cooling process, and thus, at higher

temperatures, the kinetic energy of a collisionless gas is the main contribution to the total energy. Thus, as a first approximation, particle interactions can be neglected. As the temperature decreases and the system enters a low-energy regime, interactions are governed by the scattering length a_s , which can be experimentally controlled by an external magnetic field. Thus, the interaction can be chosen to be sufficiently low that the system enters a weakly interacting regime, also known as a nearly ideal gas. In this sense, experimentally, the evaporative cooling process can be studied in an approximation in which interactions are negligible. In this form, the total energy of the gas is given by the Hamiltonian [30]:

$$H = \sum_i \left(\frac{p_i^2}{2m} + U(\mathbf{r}_i) \right), \quad (1)$$

where $p_i^2/2m$ is the kinetic energy of atom i with mass m . The momentum of the particles is $p_i = |\mathbf{p}_i|$, and $U(\mathbf{r}_i)$ is the potential energy and represents the external trap of the system.

Eq. (1) gives an expression for many particles in a macrostate. In the semiclassical limit, the Hamiltonian can be approximated to a classical form:

$$\varepsilon = H(\mathbf{r}, \mathbf{p}) = \frac{p^2}{2m} + U(\mathbf{r}) \quad (2)$$

i.e., the kinetic and potential energies are averaged over the N particles. This allows us to give a phase-space semiclassical form to the distribution functions of classical and quantum gases:

$$f^{(0)}(\varepsilon; \mu, T) = \exp \left\{ \frac{1}{k_B T} \left[\frac{p^2}{2m} + U(\mathbf{r}) - \mu \right] \right\}, \quad (3)$$

$$f^{(-)}(\varepsilon; \mu, T) = \frac{1}{\exp \left\{ \frac{1}{k_B T} \left[\frac{p^2}{2m} + U(\mathbf{r}) - \mu \right] \right\} - 1}, \quad (4)$$

$$f^{(+)}(\varepsilon; \mu, T) = \frac{1}{\exp \left\{ \frac{1}{k_B T} \left[\frac{p^2}{2m} + U(\mathbf{r}) - \mu \right] \right\} + 1}, \quad (5)$$

where k_B is the Boltzmann constant. Eq. (3) is known as the Maxwell-Boltzmann (MB) distribution and is valid for classical systems of particles. Eqs. (4) and (5) are the Bose-Einstein (BE) and Fermi-Dirac (FD) distributions, respectively, which describe quantum systems of particles. The distribution functions depend on the values of the chemical potential μ , and on the temperature T of the system.

B. Semiclassical distribution for trapped gases

The thermodynamic properties are given according to the theoretical framework presented in [31], where a generalized volume \mathcal{V} is related to the spatial extension of the gas. Experimentally, the trapped cloud

geometry depends solely on the potential's features. Naturally, if we use a semiclassical distribution, we hope to reproduce the functional forms reported in the literature and that they also have some experimental relevance. Thus, calculating thermodynamic quantities could be reduced to knowing at least two quantities: the number and the internal energy. In this sense, $f^{(a)}(\mathbf{r}, \mathbf{p})$ has the advantage that it can be integrated directly to obtain both the thermodynamic variables of classical or quantum origin [32].

Through semiclassical density distributions from (3) to (5), we can obtain some thermodynamic quantities such as the number of particles N and the internal energy E for given values of μ and T . We begin by considering a phase space cell

$$dN = \frac{1}{h^3} d^3 r d^3 p f^{(a)}(\mathbf{r}, \mathbf{p}) \quad (6)$$

and a distribution function $f^{(a)}(\epsilon; \mu, T)$, which can take the form of eq. (3) for classical ($a = 0$), eq. (4) for bosons ($a = -$), or eq. (5) for fermions ($a = +$). To simplify the notation for the distribution functions, we take

$$f^{(a)}(\mathbf{r}, \mathbf{p}; \mu, T) \equiv f^{(a)}(\epsilon; \mu, T) \equiv f^{(a)}(\mathbf{r}, \mathbf{p}).$$

It represents the phase-space occupation at point (\mathbf{r}, \mathbf{p}) ; within an elementary phase space volume $(2\pi\hbar)^{-3}$. Integrating over the phase space cell dN , we obtain the total number of particles under the distribution:

$$N = \frac{1}{(2\pi\hbar)^3} \int d^3 r \int d^3 p f^{(a)}(\mathbf{r}, \mathbf{p}). \quad (7)$$

Integrating only the phase-space density over momentum space, we find the probability of finding an atom at position \mathbf{r} ; i.e., the density distribution of the gas in position space:

$$n(\mathbf{r}) = \frac{1}{(2\pi\hbar)^3} \int d^3 p f^{(a)}(\mathbf{r}, \mathbf{p}). \quad (8)$$

Trapped clouds are strongly inhomogeneous, as the density must drop from its maximum value at the center of the cloud to the external potential minimum. Therefore, as expected, the system in an external trap has a non-homogeneous density distribution; in fact, it has a unique profile determined by the geometry of the confinement. However, this can only be observed when quantum statistics manifest, which depends strongly on temperature and the number of atoms. In fact, from the experimental point of view, at least in physics ultracold atoms, we do not have access to the density of the samples $n(\mathbf{r})$, but to the density integrated into one of the directions due to the way the data is analyzed, which is usually through a saturated absorption image [33, 34]. Despite this, it is possible to distinguish the two two-dimensional densities, and each will have a unique imprint. Thus, using the equation (8), we can rewrite the number of particles as a function of the density distribution:

$$N(\epsilon; \mu, T) = \int d^3 r n(\mathbf{r}). \quad (9)$$

Thermodynamically, the canonical relationship of conjugated entities is found through the product of chemical potential and the number of particles. This consideration leads us to conclude that $N(\epsilon; \mu, T)$ has the property of being extensive, and this quality must be maintained by definition. Therefore, it shows that, despite the sample being inhomogeneously distributed due to potential, the functional form of the number must contain information about this extensivity.

Similarly, for classical and quantum distributions in the ideal gas limit, we can find the internal energy of the system by integrating the internal energy of an individual atom in state s on phase space:

$$E(\epsilon; \mu, T) = \frac{1}{h^3} \int d^3 r \int d^3 p \left(\frac{p^2}{2m} + U(\mathbf{r}) \right) f^{(a)}(\mathbf{r}, \mathbf{p}), \quad (10)$$

In the same way, energy will also be an extensive quantity by definition, manifesting itself in the form of each external potential. Note that the expression is merely a method for calculating the average energy.

At this point, we can separate the classical gas from the quantum gas, specify their distributions, integrate them over the space of moments, and retain the explicit functional form of the number of particles as a function of the chemical potential, temperature, and potential. In this form, for classical gas, we have:

$$N(\epsilon; \mu, T) = \int d^3 r \frac{e^{\alpha(\mathbf{r})}}{\lambda^3}, \quad (11)$$

and

$$E(\epsilon; \mu, T) = \frac{3\pi\hbar^2}{m} \int d^3 r \frac{e^{\alpha(\mathbf{r})}}{\lambda^5} + \int d^3 r U(\mathbf{r}) \frac{e^{\alpha(\mathbf{r})}}{\lambda^3}. \quad (12)$$

$\lambda = (\hbar^2/2\pi mk_B T)^{1/2}$ is de Broglie thermal wavelength. On the other hand, each expression has a local fugacity of the system given by the quantity

$$e^{\alpha(\mathbf{r})} = \exp \left[\frac{1}{k_B T} (\mu - U(\mathbf{r})) \right]. \quad (13)$$

Which, at its core, contains the *local density approximation* (LDA), in which we assume density variations to be slow, in this case due to external confinement. In this form, we treat the local density as uniform, i.e., a homogeneous case modified by the external potential.

The set of thermodynamic properties for the quantum gases has a very similar procedure to obtain the number of particles

$$N(\epsilon_s; \mu, T) = \int d^3 r \frac{g_{3/2}^{(\pm)}(\alpha(\mathbf{r}))}{\lambda^3} \quad (14)$$

and the energy

$$E(\epsilon_s; \mu, T) = \frac{3\pi\hbar^2}{m} \int d^3 r \frac{g_{5/2}^{(\pm)}(\alpha(\mathbf{r}))}{\lambda^5} + \int d^3 r U(\mathbf{r}) \frac{g_{3/2}^{(\pm)}(\alpha(\mathbf{r}))}{\lambda^3}, \quad (15)$$

where the function $g_s^{(\pm)}$ denotes a s -order polylogarithm, whose the integral form is:

$$g_s^{(\pm)}(\alpha) = \frac{1}{\Gamma(v)} \int_0^\infty dx \frac{x^{s-1}}{e^{x-\alpha} \mp 1}. \quad (16)$$

The sign of $g_s^{(\pm)}$ corresponds to the FD(-) or the BE (+) distributions.

C. Thermodynamic variables for confining potentials

The confining external potentials considered in this work for studying the thermodynamics of the cooling evaporation process are listed in Table I. The external potentials can generally be written as $U \equiv U(x, y, z, l_x, l_y, l_z)$, where the parameters l_i do not necessarily have length units. Each confining potential has its generalized volume (\mathcal{V}) variable (see Table I). It also does not necessarily have a volume unit and is considered an extensive quantity because it relates to the gas's spatial extent within the atomic trap.

The boundaries of the box potentials in different dimensions are given by:

$$U_{1D} = \begin{cases} 0 & r \in L \\ \infty & \notin L \end{cases}, \quad U_{2D} = \begin{cases} 0 & r \in S \\ \infty & \notin S \end{cases}, \quad U_{3D} = \begin{cases} 0 & r \in V \\ \infty & \notin V \end{cases}. \quad (17)$$

Thus, each box potential is defined in a line L , a surface S , and a volume V , respectively. In the same way, we can have harmonic confinements in one, two, and three dimensions. However, it should be noted that one of the main interests of this article is the anisotropic three-dimensional harmonic potential, that is, when $\omega_x \neq \omega_y \neq \omega_z$ since essentially all potentials used experimentally are of this class.

We are inspired by potential designs, especially those related to homogeneous gases, as different experimental realizations have been performed using potentials that can be considered mixed, combining harmonic and box-type potentials. They have been of great importance for the approach to two-dimensional physics since they have been obtained for both Bose [21, 22] and Fermi gases [23, 24]. In addition, we can propose the combination of two potentials, the harmonic and the box potential, whose generalized volumes are shown in Table I.

TABLE I. Constants and global volumes for each potential.

Potential	$U(\mathbf{r})$	\mathcal{V}	K	ν
3D-Box	$U_{3D}(x, y, z)$	V	$(\frac{m}{2\pi})^{3/2}$	3
2D-Box + 1D-HO	$U_{2D}(x, y) + \frac{1}{2}m\omega_z^2 z^2$	$S(\omega_z)^{-1}$	$(\frac{m}{2\pi})^2$	4
1D-Box + 2D-HO	$U_{1D}(z) + \frac{1}{2}m(\omega_x^2 x^2 + \omega_y^2 y^2)$	$L(\omega_y \omega_x)^{-1}$	$(\frac{m}{2\pi})^{5/2}$	5
3D-HO	$\frac{1}{2}m(\omega_x^2 x^2 + \omega_y^2 y^2 + \omega_z^2 z^2)$	$(\omega_x \omega_y \omega_z)^{-1}$	1	6
Quadrupole	$\sqrt{(A_x x)^2 + (A_y y)^2 + (A_z z)^2}$	$(A_x A_y A_z)^{-1}$	$8\pi(\frac{m}{2\pi})^{3/2}$	9

We can open a parenthesis to explore the idea of the number of degrees of freedom of a gas, which we label with the Greek letter ν (see Table I). Strictly speaking, we have the three spatial degrees of freedom of movement as seen in the “pure box” potential, and as we add the degrees of freedom of the confinement field, that is, curvatures associated with the harmonic potential, ν increases until we find its maximum in the “pure oscillator”. In this sense, harmonic confinement doubles the degrees of freedom of the box confinement (free gas with walls).

A special case is the linear quadrupole trap, widely used in experiments that begin their evaporation in a purely magnetic trap. As is well known, from an experimental point of view, it has a technical problem due to the zero field and to leakage of colder atoms. However, it is interesting because at high temperatures, the potential has a larger phase space, allowing faster thermalization in evaporative cooling. Usually, the geometric scale is given in terms of the gradient of the potential (B') in the strongest direction of the magnetic potential:

$$\mu_B B' = A_x = A_y = 2A_z,$$

where μ_B is the Bohr magneton. From the physical point of view, in this potential, the notion of the degrees of freedom of the particle is lost, although we will refer to ν as the degrees of freedom, although they will no longer correspond to these.

As expected, we can analytically determine both the number and the energy of classical and quantum gases. Furthermore, it will serve as our primary tool to show the differences as we approach degeneration temperatures. Without any more preambles, the general forms for the number or particles are:

$$N = K \frac{\mathcal{V}}{\hbar^3} (k_B T)^{\nu/2} e^{\alpha}, \quad N = K \frac{\mathcal{V}}{\hbar^3} (k_B T)^{\nu/2} g_{\nu/2}^{(\pm)}(\alpha), \quad (18)$$

for the classical and quantum gases, respectively. K is reported in Table I for each considered potential. In a similar form for the energy:

$$E = \frac{\nu}{2} N k_B T, \quad E = \frac{\nu}{2} N k_B T \frac{g_{\nu/2+1}^{(\pm)}(\alpha)}{g_{\nu/2}^{(\pm)}(\alpha)} \quad (19)$$

The equipartition theorem states that the average internal energy of a system of N particles is given by $E/N = \nu k_B T / 2$, where ν represents the degrees of freedom[35].

III. EVAPORATIVE COOLING

In ultracold matter, evaporative cooling [17, 36] is one of the most used experimental techniques for achieving low temperatures below the recoil and sub-Doppler limit for dilute gases. This method reduces

the depth of the external potential. As a result, atoms are selectively removed in the high-energy state of the thermal distribution. Through collisions among the remaining atoms, the system undergoes rethermalization. Due to its importance, theoretical studies of this procedure have been reported [37, 38]. In both references, evaporative cooling is modeled as a discrete process arising from truncating the energy distribution, which is assumed to follow the classical MB distribution.

In this work, we not only consider the MB distribution but also introduce the quantum distributions of FD and BE, allowing us to observe variations in thermodynamic behavior during evaporation, including thermodynamic equilibrium states. As discussed below and as expected, the behavior of the three distributions differs significantly at low temperatures. In the opposite case, the gases behave similarly at higher temperatures, as expected for classical systems in this regime. For bosons, the value of this critical temperature to reach quantum degeneracy depends on the external confined potential. For us, a special interest lies in the quadrupole potential, which exhibits distinct behavior across the three distributions considered in this work.

We present the main results of our work on the theoretical model in the sections below.

A. Evaporative cooling protocol

We have access to the initial particle number, the energy, and the sample's initial temperature. We can obtain these quantities directly from any distributions posed in equations (3)-(5). As mentioned above, the functional form of the distributions will depend on the form of the external potential $U(\mathbf{r})$ (embedded in ϵ). We label the initial temperature with the index 0; in this way, given a temperature T_0 and a chemical potential μ_0 , we can calculate the number of particles and the energy:

$$N_0 = \frac{1}{h^3} \int d^3r \int d^3p f_0^{(a)}(\epsilon; \mu_0, T_0), \quad (20)$$

$$E_0 = \frac{1}{h^3} \int d^3r \int d^3p \left(\frac{p^2}{2m} + U(\mathbf{r}) \right) f_0^{(a)}(\epsilon; \mu_0, T_0). \quad (21)$$

$a = 0, \pm$, for MB, BE, and FD distributions, respectively. Note that these expressions are general.

So, given a distribution, it is possible to define a temperature at which we are going to cut and, therefore, a 'cut-off' momentum q_c ; in this sense, all particles with an associated momentum greater than q_c will be removed. The cut-off moment also has an associated energy $\epsilon_c = q_c^2/2m$, and we choose this cut-off reasonably to maintain adiabaticity. This means we cannot make abrupt cuts, since we are discussing systems near equilibrium at each cut. Otherwise, we would enter the field of phenomena outside equilibrium and, therefore, thermodynamics that does not correspond to the objectives of this article.

The schematic representation of the mentioned process is shown in Fig. 1. Before removing the particles,

the gas is in an equilibrium initial state characterized by the variables- (N_0, E_0) (Fig. 1(a)); after the cut-off (Fig. 1(b)), the system reaches a new set of variables- (N_1^c, E_1^c) (Fig. 1(c)). The new set is a function of initial conditions, T_0 and μ_0 . In other words, we choose the distribution but by a truncated integral in the momentum space of the original distribution. Remember that we must remove the hottest atoms; in this sense, the truncated integral represents just that.

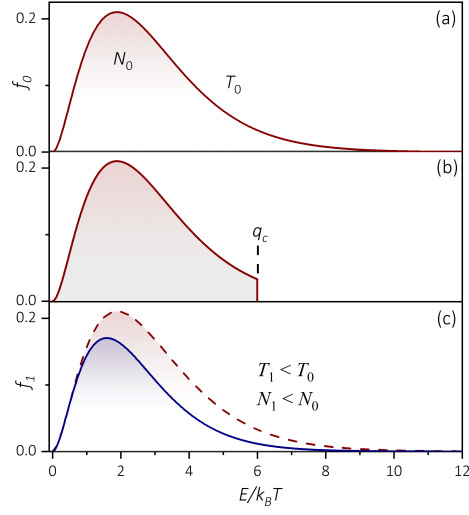


FIG. 1. Scheme protocol of evaporation. (a) We start with a gas distribution at temperature T_0 and with N_0 atoms. Then, (b) a cut is made in said distribution, discarding those higher-energy atoms. After this process, (c) the system re-thermalizes to a new temperature, T_1 , and a new number, N_1 , where both will be lower than the initial conditions.

The procedure for truncating the integrals will be analogous for both classical and quantum distributions.

We can start the cut-off for the number of atoms in the MB distribution

$$\begin{aligned}
 & N_1^c(\epsilon_s, \mu_0, T_0) \\
 &= \frac{4\pi}{h^3} \int d^3 r \int_0^{q_c} dp p^2 f_0^{(0)}(\epsilon; \mu_0, T_0) \\
 &= \left\{ \operatorname{erf}[\sqrt{\eta_0}] - \frac{2}{\sqrt{\pi}} \sqrt{\eta_0} e^{-\eta_0} \right\} \int d^3 r \frac{e^{\alpha_0(\mathbf{r})}}{\lambda_0^3}, \tag{22}
 \end{aligned}$$

and quantum distributions are

$$\begin{aligned}
 & N_1^c(\epsilon_s, \mu_0, T_0) \\
 &= \frac{4\pi}{h^3} \int d^3 r \int_0^{q_c} dp p^2 f_0^{(\pm)}(\epsilon; \mu_0, T_0) \\
 &= \frac{1}{\lambda_0^3} \sum_{j=1}^{\infty} (\pm 1)^{j+1} \int d^3 r \frac{e^{j\alpha_0(\mathbf{r})}}{j^{3/2}} \operatorname{erf}[\sqrt{j\eta_0}] \\
 &- \frac{q_c}{\pi \hbar} \frac{1}{\lambda_0^2} \sum_{j=1}^{\infty} (\pm 1)^{j+1} \int d^3 r \frac{e^{j(\alpha_0(\mathbf{r}) - \eta_0)}}{j}, \tag{23}
 \end{aligned}$$

where

$$\alpha_0(\mathbf{r}) = \frac{1}{k_B T_0} (\mu_0 - U(\mathbf{r})), \quad \eta_0 = \frac{q_c^2}{2mk_B T_0}, \quad (24)$$

and

$$\operatorname{erf}[\sqrt{\eta}] = \frac{2}{\sqrt{\pi}} \int_0^\eta dt e^{-t^2}, \quad (25)$$

where the last one is the error function.

On the other hand, we have the energies associated with truncated functions for classical

$$\begin{aligned} & E_1^c(\varepsilon_s, \mu_0, T_0) \\ &= \frac{4\pi}{h^3} \int d^3 r \int_0^{q_c} dp p^2 \left(\frac{p^2}{2m} + U(\mathbf{r}) \right) f_0^{(0)}(\varepsilon; \mu_0, T_0) \\ &= \frac{e^{-\eta_0}}{\lambda_0^2} \left\{ \frac{3\pi\hbar^2 \operatorname{erf}[\sqrt{\eta_0}]}{m \lambda_0^3 e^{-\eta_0}} - \frac{3q_c \hbar}{m \lambda_0^2} - \frac{q_c^3}{2\pi m \hbar} \right\} \int d^3 r e^{\alpha_0(\mathbf{r})} \\ &+ \frac{e^{-\eta_0}}{\lambda_0^2} \left\{ \frac{\operatorname{erf}[\sqrt{\eta_0}]}{\lambda_0 e^{-\eta_0}} - \frac{q_c}{\pi \hbar} \right\} \int d^3 r U(\mathbf{r}) e^{\alpha_0(\mathbf{r})}, \end{aligned} \quad (26)$$

and quantum distributions

$$\begin{aligned} & E_1^c(\varepsilon_s, \mu_0, T_0) \\ &= \frac{4\pi}{h^3} \int d^3 r \int_0^{q_c} dp p^2 \left(\frac{p^2}{2m} + U(\mathbf{r}) \right) f_0^{(\pm)}(\varepsilon; \mu_0, T_0) \\ &= \frac{3\pi\hbar^2}{m} \frac{1}{\lambda_0^5} \sum_{j=1}^{\infty} (\pm 1)^{j+1} \int d^3 r \frac{e^{j\alpha_0(\mathbf{r})}}{j^{5/2}} \operatorname{erf}[\sqrt{j\eta_0}] \\ &- \frac{3q_c \hbar}{m} \frac{1}{\lambda_0^4} \sum_{j=1}^{\infty} (\pm 1)^{j+1} \int d^3 r \frac{e^{j(\alpha_0(\mathbf{r}) - \eta_0)}}{j^2} \\ &- \frac{q_c^3}{2\pi m \hbar} \frac{1}{\lambda_0^2} \sum_{j=1}^{\infty} (\pm 1)^{j+1} \int d^3 r \frac{e^{j(\alpha_0(\mathbf{r}) - \eta_0)}}{j} \\ &+ \frac{1}{\lambda_0^3} \sum_{j=1}^{\infty} (\pm 1)^{j+1} \int d^3 r U(\mathbf{r}) \frac{e^{j\alpha_0(\mathbf{r})}}{j^{3/2}} \operatorname{erf}[\sqrt{j\eta_0}] \\ &- \frac{q_c}{\pi \hbar} \frac{1}{\lambda_0^2} \sum_{j=1}^{\infty} (\pm 1)^{j+1} \int d^3 r U(\mathbf{r}) \frac{e^{j(\alpha_0(\mathbf{r}) - \eta_0)}}{j}. \end{aligned} \quad (27)$$

Moreover $\lambda_0 = (h^2/2\pi m k_B T_0)^{1/2}$, is the de Broglie thermal wavelength for T_0 .

Once the system distributes its energy E_1 , it is rethermalized at a new temperature T_1 . Then, the system will also have a new chemical potential, μ_1 , that fixes the number of particles, N_1 . In this sense, the gas reaches a new equilibrium situation, as the energy cut is significantly smaller than the total energy. Thus, once the gas reaches the new temperature and the new number, we have a new distribution $f_1^{(a)}(\varepsilon, \mu_1, T_1)$, and we can rewrite the expressions as:

$$N_1^c(\mu_0, T_0) = N_1(\mu_1, T_1), \quad E_1^c(\mu_0, T_0) = E_1(\mu_1, T_1). \quad (28)$$

Note that both the energy and the number of particles are functions of T_1 and μ_1 , which leads us to conclude that we can invert the expressions. The inversion is an enormous effort from the analytical point of view, but not so much from the numerical point of view. Finally, we have:

$$T_1 = T_1(N_1, E_1), \quad \mu_1 = \mu_1(N_1, E_1), \quad (29)$$

which are 2×2 non-linear system of equations that can be solved for T_1 and μ_1 . It should be noted that all equations explicitly depend on the external variable \mathcal{V} ; however, since we are considering the potential to be fixed, this variable will disappear when rewriting the equations in terms of the initial quantities. This fact will be reflected in the following sections.

B. Applied evaporative cooling protocol

The key to successfully implementing evaporative cooling is the ability to convert the expressions in equations (22)–(27) into a discretized, recursive form. This transformation allows one to systematically relate the initial thermodynamic variables, i.e. energy (E_0), particle number (N_0), chemical potential (μ_0), and temperature (T_0), to their corresponding final values (E_1, N_1, μ_1, T_1) after a cooling step, while selecting the appropriate functional form of the potential[39].

The process begins by specifying the system's initial thermodynamic state, characterized by the set (N_0, E_0, T_0, μ_0) , along with an initial cut-off momentum value, denoted q_c . This cut-off momentum defines an initial energy threshold, η_0 , above which particles are removed. To simulate evaporative cooling, particles with energies exceeding a new, lower cut-off energy $\eta_1 = \eta_0 - \Delta\eta$ are removed from the system. This step corresponds to a controlled, linear reduction in temperature.

Following particle removal, the system is allowed to rethermalize, reaching a new equilibrium state described by updated thermodynamic quantities (N_1, E_1, T_1, μ_1) . This cycle of lowering the energy cut-off, removing particles, and rethermalizing can be repeated. The procedure continues until a target critical temperature T_c is reached, as in the case of bosonic gases undergoing BE condensation, or until the particle population is exhausted.

This discretized, recursive approach provides a practical framework to model the dynamics of evaporative cooling, capturing both the gradual loss of high-energy particles and the resulting changes in thermodynamic properties at each step. These relations form a set of recurrence equations that can be generalized to compute the thermodynamic quantities of a gas that has lost its hottest particles in the i -th step as a function of the thermodynamic quantities from the previous $(i - 1)$ -th step. In other words, the initial equilibrium state, labeled as step zero, can be mapped to the i -th step, while the variables labeled one correspond to

the $(i - 1)$ -th step. Once the explicit forms of equations (22)–(27) are determined, this protocol applies universally to any distribution function, whether classical or quantum.

From the potentials presented in Table I, we applied the protocol to systems confined by the 3D-Box ($\nu = 3$), 3D-HO ($\nu = 6$), and quadrupole ($\nu = 9$). We find a set of general recurrence relations for the classical gas

$$\frac{N_i}{N_{i-1}} = \text{erf}[\sqrt{\eta_{i-1}}] - \frac{2}{\sqrt{\pi}} \eta_{i-1}^{1/2} e^{-\eta_{i-1}}, \quad (30)$$

$$\frac{E_i}{E_{i-1}} = \frac{4x}{\nu} \text{erf}[\sqrt{\eta_{i-1}}] - \frac{2}{\sqrt{\pi}} \eta_{i-1}^{1/2} e^{-\eta_{i-1}} - \frac{4}{\nu\sqrt{\pi}} \eta_{i-1}^{3/2} e^{-\eta_{i-1}}. \quad (31)$$

where $x = 3/2, 3, 3$, for 3D-box, 3D-HO, and quadrupole, respectively. It is worth mentioning that these results are in complete agreement with those presented for classical gases by Henn et al. [37] and Davis et al. [38].

The recurrences for quantum gases are slightly complicated but compact forms:

$$\frac{N_i}{N_{i-1}} = \frac{\tilde{g}_{\nu/2}^{(\pm)}(\alpha_{i-1}, \eta_{i-1})}{g_{\nu/2}^{(\pm)}(\alpha_{i-1})} - \frac{2}{\sqrt{\pi}} \eta_{i-1}^{1/2} \frac{\tilde{g}_{\nu/2-1}^{(\pm)}(\alpha_{i-1}, \eta_{i-1})}{g_{\nu/2}^{(\pm)}(\alpha_{i-1})}, \quad (32)$$

$$\begin{aligned} \frac{E_i}{E_{i-1}} &= \frac{\tilde{g}_{\nu/2+1}^{(\pm)}(\alpha_i, \eta_{i-1})}{g_{\nu/2+1}^{(\pm)}(\alpha_{i-1})} - \frac{2}{\sqrt{\pi}} \eta_{i-1}^{1/2} \frac{\tilde{g}_{\nu/2+1/2}^{(\pm)}(\alpha_{i-1}, \eta_{i-1})}{g_{\nu/2+1}^{(\pm)}(\alpha_{i-1})} \\ &- \frac{4}{\nu\sqrt{\pi}} \eta_{i-1}^{3/2} \frac{\tilde{g}_{\nu/2-1}^{(\pm)}(\alpha_{i-1}, \eta_{i-1})}{g_{\nu/2+1}^{(\pm)}(\alpha_{i-1})}. \end{aligned} \quad (33)$$

For the results presented before, following the quantities:

$$\eta_i = \frac{\varepsilon_c}{k_B T_i} = \frac{q_c^2}{2mk_B T_i}, \quad \alpha_i = \frac{\mu_i}{k_B T_i}. \quad (34)$$

As mentioned above, the recurrence relations are not dependent on extensive variables (\mathcal{V}). However, to feed the protocol's first data, we conveniently choose a specific value for each potential $U(\mathbf{r})$ of interest.

On the other hand, we define $\tilde{g}_s^{(\pm)}(\alpha, \sigma)$ and $\tilde{g}_s^{(\pm)}(\alpha, \sigma)$ as modified Bose-Einstein and FD distributions.

The bar functions have the following form:

$$\tilde{g}_s^{(\pm)}(\alpha, \sigma) = \sum_{j=1}^{\infty} (\pm 1)^{j+1} \frac{e^{j(\alpha-\sigma)}}{j^s}, \quad (35)$$

where an interesting limit is: $\lim_{\sigma \rightarrow \infty} \tilde{g}_s^{(\pm)}(\alpha, \sigma) = 0$. In the same form, for the tilde-function:

$$\tilde{g}_s^{(\pm)}(\alpha, \sigma) = \sum_{j=1}^{\infty} (\pm 1)^{j+1} \frac{e^{j\alpha}}{j^s} \text{erf}[\sqrt{j\sigma}], \quad (36)$$

we have the follow limit $\lim_{\sigma \rightarrow \infty} \tilde{g}_s^{(\pm)}(\alpha, \sigma) = g_s^{(\pm)}(\alpha)$, the usual functions. The behavior in this limit arises because the error function quickly saturates to 1 for very large arguments.

IV. NUMERICAL RESULTS AND DISCUSSION

In this section, we analyze the evaporative cooling process for the MB, FD, and BE statistical distributions in the presence of three distinct external potentials: a 3D box, a harmonic oscillator, and a quadrupole trap (Figure 2). For each potential, two graphs are presented. On the left side of Figure 2, we show the N vs. T curves for an initial temperature of 50 mK, 1×10^7 particles, and an initial cut-off energy of $\eta_0 = 0.5 \mu\text{K}$, using a fixed step of $\Delta\eta = 0.1 \mu\text{K}$. The graph on the right illustrates the evaporation curve typically observed in experiments, where a linear decrease in the cut-off energy results in a reduction in the number of trapped atoms. Experimentally, this cut-off is implemented either by lowering the intensity of the confining potential or by inducing transitions with radio-frequency fields. In all cases, the left-hand graph highlights the relationship between the thermodynamic variables, specifically, the number of atoms and the sample temperature, throughout the evaporation process.

Equations (30)–(33) define a set of recurrence relations used to compute the thermodynamic quantities that characterize the system. Notably, these relations do not yield analytical expressions for either the temperature or the chemical potential, which necessitates a numerical approach. By applying the Newton–Raphson method [40] to solve a 2×2 system of non-linear equations with temperature T_1 and chemical potential μ_1 as variables, determined by the number of particles N_1 and the energy E_1 , we obtain a numerical solution. Combined with Eq. (27), this solution can be generalized in the same manner as previously discussed. Furthermore, by iterating this procedure within the evaporative cooling protocol, we can analyze the thermodynamic evolution of the system for each potential described in Section III B.

At the initial stages of the evaporative cooling process, the FD and BE distributions exhibit behavior similar to that of the classical MB distribution. However, as the sample temperature decreases, the system’s quantum nature becomes increasingly significant. As previously discussed, the bosonic system undergoes a phase transition, leading to BE condensation. In contrast, at sufficiently low temperatures, the FD gas exhibits effective heating behavior, a consequence of the Pauli exclusion principle and the associated modification of its energy distribution.

Evaporative cooling is employed to reach the degeneracy regime in an interacting atomic sample. For bosonic atoms, entering this regime leads to a superfluid transition and the formation of a BE condensate. Numerical simulations of evaporative cooling for a gas obeying BE statistics are therefore expected to reproduce this behavior. Fig. 2 illustrates the onset of condensation for a bosonic gas confined in a linear quadrupolar potential. When the gas temperature approaches 1.25×10^{-5} K, the number of atoms in the system stabilizes, and the sample temperature no longer decreases. A similar trend is observed for the 3D box and harmonic oscillator potentials (Fig. 2), where evaporative cooling effectively stops at approximately

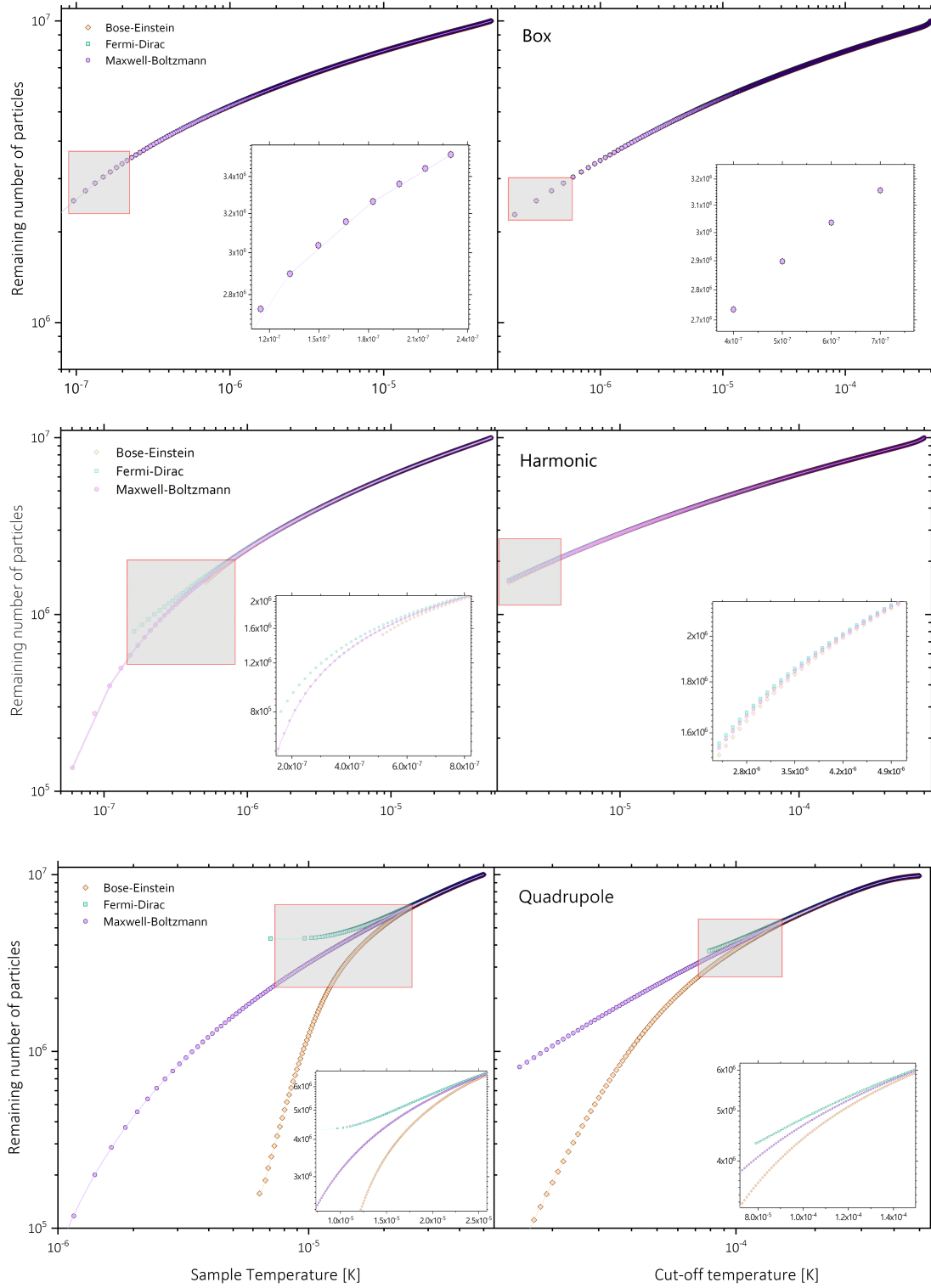


FIG. 2. Sample temperature is a function of the cut-off energy for a system confined in a box, harmonic, and quadrupole potential. They all have an initial temperature of $50\mu\text{K}$, a cut-off energy of $\eta_0 = 0.5\text{mK}$, and a fixed step of $\Delta\eta = 0.1\mu\text{K}$.

1×10^{-7} K and 5×10^{-7} K, respectively. These temperatures are consistent with the experimentally reported critical values for BE condensation in these external potentials, assuming an ideal gas.

Numerically, condensation is identified when the chemical potential reaches zero, causing the polylogarithmic function in the Bose–Einstein distribution to become constant. For positive chemical potentials, the polylogarithm diverges, preventing condensation. Although Fig. 2 shows the condensation of a Bose gas in a linear quadrupolar potential, this configuration is experimentally challenging due to Majorana losses [41]. In such traps, atoms tend to escape at the point where the quadrupolar magnetic field vanishes, making stable confinement difficult to achieve.

For MB statistics, we observe that the evaporative cooling process behaves as expected for an ideal gas with no internal degrees of freedom (i.e., no interactions) across the three external potentials considered. As the energy cut-off is progressively lowered, the number of atoms in the system decreases smoothly until it reaches zero. Although Fig. 2 do not explicitly display this limit, no physical mechanism prevents the complete removal of all atoms, in contrast to the cases governed by FD and BE statistics. Another notable feature is the remarkable similarity in the Maxwell–Boltzmann behavior across the three external potentials. This uniformity arises from the absence of quantum correlations, which fundamentally distinguishes classical from quantum statistics.

The behavior of the temperature loss is also linked to the system’s degrees of freedom. When more degrees of freedom are present, as in the quadrupolar potential, the onset of differentiation among the three statistics appears at higher temperatures. In the quadrupolar trap, which effectively has nine degrees of freedom, the three distributions behave identically at high temperatures, where the system remains fully classical. As the temperature decreases and the number of particles is reduced, the statistical behavior begins to diverge, with the separation becoming evident around 2.5×10^{-5} K in the sample temperature.

V. CONCLUSIONS

In summary, this article presents a semiclassical framework that unifies the evaporative cooling process for classical and quantum gases under a variety of external confining potentials. By introducing generalized thermodynamic variables and deriving recurrence relations for the particle number and internal energy, we demonstrated that the evaporation dynamics can be fully characterized at each step of the cooling protocol. Our results show that the statistical nature of the gas plays a decisive role in determining the efficiency and limits of evaporative cooling. In particular, the polylogarithmic structure of the BE and FD distributions captures the emergence of quantum degeneracy, the onset of BE condensation, and the effective heating observed in fermionic systems at low temperatures. Moreover, the external potential alters the order of the

polylogarithm, thereby influencing the temperature-loss rate and the evolution of the particle number during cooling.

The numerical implementation of the protocol across different trapping geometries, including the 3D box, the harmonic oscillator, and the quadrupole trap, reveals how the degrees of freedom associated with each potential shape the thermodynamic trajectories during evaporation. While MB gases exhibit a smooth, complete depletion of particles, quantum gases display distinct degeneracy signatures that depend sensitively on both temperature and trap geometry. The framework presented here provides a versatile tool for modeling evaporative cooling in experimentally relevant configurations, offering insights into the interplay between confinement, statistics, and thermodynamic evolution. Future extensions may incorporate interaction effects, non-equilibrium dynamics, or time

One of the most important results of our study is that the system's statistical nature directly influences the evaporation process. Although particle interactions are not included, the polylogarithmic functions associated with the FD and BE distributions accurately reproduce the system's equilibrium behavior. Furthermore, the external potential modifies the order ν of the polylogarithm, thereby affecting both the rate of temperature loss and the evolution of the particle number throughout the cooling process.

-
- [1] L. Luo, B. Clancy, J. Joseph, J. Kinast, A. Turlapov, and J. E. Thomas, Evaporative cooling of unitary fermi gas mixtures in optical traps, *New J. Phys.* **8**, 213 (2006).
 - [2] K. B. Davis, M.-O. Mewes, M. A. Joffe, M. R. Andrews, and W. Ketterle, Evaporative cooling of sodium atoms, *Phys. Rev. Lett.* **74**, 5202 (1995).
 - [3] M. H. Anderson, J. R. Ensher, M. R. Matthews, C. E. Wieman, and E. A. Cornell, Observation of bose-einstein condensation in a dilute atomic vapor, *Science* **269**, 198 (1995).
 - [4] M. D. Barrett, J. A. Sauer, and M. S. Chapman, All-optical formation of an atomic bose-einstein condensate, *Phys. Rev. Lett.* **87**, 010404 (2001).
 - [5] M. Holland, J. Williams, and J. Cooper, Bose-einstein condensation: Kinetic evolution obtained from simulated trajectories, *Phys. Rev. A* **55**, 3670 (1997).
 - [6] A. Camacho-Guardian, M. Mendoza-López, V. Romero-Rochín, and R. Paredes, Energetic cooling below the bec transition: a quantum kinetic description within the bogoliubov approximation, *J. Phys. B: Atomic, Molecular and Optical Physics* **47**, 215304 (2014).
 - [7] M. Yamashita, M. Koashi, and N. Imoto, Quantum kinetic theory for evaporative cooling of trapped atoms: Growth of bose-einstein condensate, *Phys. Rev. A* **59**, 2243 (1999).
 - [8] O. J. Luiten, M. W. Reynolds, and J. T. M. Walraven, Kinetic theory of the evaporative cooling of a trapped gas, *Phys. Rev. A* **53**, 381 (1996).
 - [9] I. Bloch, J. Dalibard, and S. Nascimbène, Quantum simulations with ultracold quantum gases, *Nature Phys.* **8**,

- 267 (2012).
- [10] I. Bloch, J. Dalibard, and W. Zwerger, Many-body physics with ultracold gases, *Rev. Mod. Phys.* **80**, 885 (2008).
 - [11] W. Hofstetter and T. Qin, Quantum simulation of strongly correlated condensed matter systems, *J. Phys. B: At., Mol. Opt. Phys.* **51**, 082001 (2018).
 - [12] E. A. Cornell and C. E. Wieman, Nobel lecture: Bose-einstein condensation in a dilute gas, the first 70 years and some recent experiments, *Rev. Mod. Phys.* **74**, 875 (2002).
 - [13] W. Ketterle, Nobel lecture: When atoms behave as waves: Bose-einstein condensation and the atom laser, *Rev. Mod. Phys.* **74**, 1131 (2002).
 - [14] R. Grimm, M. Weidemüller, Y. B. Ovchinnikov, B. Bederson, and H. Walther, Optical dipole traps for neutral atoms, in *Advances In Atomic, Molecular, and Optical Physics*, Vol. 42 (Academic Press, 2000) pp. 95–170.
 - [15] D. M. Stamper-Kurn, M. R. Andrews, A. P. Chikkatur, S. Inouye, H.-J. Miesner, J. Stenger, and W. Ketterle, Optical confinement of a bose-einstein condensate, *Phys. Rev. Lett.* **80**, 2027 (1998).
 - [16] S. R. Granade, M. E. Gehm, K. M. O’Hara, and J. E. Thomas, All-optical production of a degenerate fermi gas, *Phys. Rev. Lett.* **88**, 120405 (2002).
 - [17] K. B. Davis, M. O. Mewes, M. R. Andrews, N. J. van Druten, D. S. Durfee, D. M. Kurn, and W. Ketterle, Bose-einstein condensation in a gas of sodium atoms, *Phys. Rev. Lett.* **75**, 3969 (1995).
 - [18] M.-S. Heo, J.-y. Choi, and Y.-i. Shin, Fast production of large ^{23}Na bose-einstein condensates in an optically plugged magnetic quadrupole trap, *Phys. Rev. A* **83**, 013622 (2011).
 - [19] D. Dudley, W. M. Duncan, and J. Slaughter, Emerging digital micromirror device (dmd) applications (2003).
 - [20] G. Gauthier, I. Lenton, N. McKay Parry, M. Baker, M. J. Davis, H. Rubinsztein-Dunlop, and T. W. Neely, Direct imaging of a digital-micromirror device for configurable microscopic optical potentials, *Optica* **3**, 1136 (2016).
 - [21] S. P. Rath, T. Yefsah, K. J. Günter, M. Cheneau, R. Desbuquois, M. Holzmann, W. Krauth, and J. Dalibard, Equilibrium state of a trapped two-dimensional bose gas, *Phys. Rev. A* **82**, 013609 (2010).
 - [22] T. Yefsah, R. Desbuquois, L. Chomaz, K. J. Günter, and J. Dalibard, Exploring the thermodynamics of a two-dimensional bose gas, *Phys. Rev. Lett.* **107**, 130401 (2011).
 - [23] K. Martiyanov, V. Makhalov, and A. Turlapov, Observation of a two-dimensional fermi gas of atoms, *Phys. Rev. Lett.* **105**, 030404 (2010).
 - [24] K. Hueck, N. Luick, L. Sobirey, J. Siegl, T. Lompe, and H. Moritz, Two-dimensional homogeneous fermi gases, *Phys. Rev. Lett.* **120**, 060402 (2018).
 - [25] V. Romero-Rochín, Equation of state of an interacting bose gas confined by a harmonic trap: The role of the “harmonic” pressure, *Phys. Rev. Lett.* **94**, 130601 (2005).
 - [26] V. Romero-Rochín and V. S. Bagnato, Thermodynamics of an ideal gas of bosons harmonically trapped: Equation of state and susceptibilities, *Braz. J. Phys.* **35**, 607 (2005).
 - [27] V. Romero-Rochín, R. F. Shiozaki, M. Caracanhas, E. A. L. Henn, K. M. F. Magalhaes, G. Roati, and V. S. Bagnato, Observation of bose–einstein condensation in an atomic trap in terms of macroscopic thermodynamic parameters, *Phys. Rev. A* **85**, 023632 (2012).
 - [28] F. J. Poveda-Cuevas, P. C. M. Castilho, E. D. Mercado-Gutierrez, A. R. Fritsch, S. R. Muniz, E. Lucioni,

- G. Roati, and V. S. Bagnato, Isothermal compressibility determination across Bose-Einstein condensation, *Phys. Rev. A* **92**, 013638 (2015).
- [29] E. D. Mercado-Gutiérrez, F. J. Poveda-Cuevas, and V. S. Bagnato, Thermal global expansion coefficient measurement for a harmonic trapped gas across bose-einstein condensation, *Braz. J. Phys.* **48**, 539 (2018).
- [30] P. W. Courteille, V. S. Bagnato, and V. I. Yukalov, Bose-einstein condensation of trapped atomic gases, *Laser Phys.* **11**, 659 (2001).
- [31] N. Sandoval-Figueroa and V. Romero-Rochín, Thermodynamics of trapped gases: generalized mechanical variables, equation of state, and heat capacity, *Phys. Rev. E* **78**, 061129 (2008).
- [32] S. Giorgini, L. P. Pitaevskii, and S. Stringari, Thermodynamics of a trapped bose-condensed gas, *Journal of Low Temperature Physics* **109**, 309 (1997).
- [33] S. R. Ramanathan, A. Muniz, K. C. Wright, R. P. Anderson, W. D. Phillips, K. Helmerson, and G. K. Campbell, Partial-transfer absorption imaging: A versatile technique for optimal imaging of ultracold gases, *Rev. Sci. Instr.* **83**, 083119 (2012).
- [34] R. Szczepkowski, J. Gartman, M. Witkowski, L. Tracewski, M. Zawada, and W. Gawlik, Analysis and calibration of absorptive images of Bose–Einstein condensate at nonzero temperatures, *Rev. Sci. Instr.* **80**, 053103 (2009).
- [35] Although this does not strictly represent all external potentials.
- [36] H. F. Hess, Evaporative cooling of magnetically trapped and compressed spin-polarized hydrogen, *Phys. Rev. B* **34**, 3476 (1986).
- [37] E. A. L. Henn, J. A. Seman, E. R. F. Ramos, A. H. Iavaronni, T. Amthor, and V. S. Bagnato, Evaporation in atomic traps: A simple approach, *Am. J. Phys.* **75**, 907 (2007).
- [38] K. B. Davis, M. O. Mewes, and W. Ketterle, An analytical model for evaporative cooling of atoms, *App. Phys. B* **60**, 155 (1995).
- [39] As defined in section II C, which satisfies the required properties.
- [40] A. Ostrowski, P. Smith, and S. Eilenberg, *Solution of Equations and Systems of Equations: Pure and Applied Mathematics: A Series of Monographs and Textbooks, Vol. 9*, v. 9 (Elsevier Science, 2016).
- [41] D. M. Brink and C. V. Sukumar, Majorana spin-flip transitions in a magnetic trap, *Phys. Rev. A* **74**, 035401 (2006).